

RSC Advances



This is an *Accepted Manuscript*, which has been through the Royal Society of Chemistry peer review process and has been accepted for publication.

Accepted Manuscripts are published online shortly after acceptance, before technical editing, formatting and proof reading. Using this free service, authors can make their results available to the community, in citable form, before we publish the edited article. This *Accepted Manuscript* will be replaced by the edited, formatted and paginated article as soon as this is available.

You can find more information about *Accepted Manuscripts* in the [Information for Authors](#).

Please note that technical editing may introduce minor changes to the text and/or graphics, which may alter content. The journal's standard [Terms & Conditions](#) and the [Ethical guidelines](#) still apply. In no event shall the Royal Society of Chemistry be held responsible for any errors or omissions in this *Accepted Manuscript* or any consequences arising from the use of any information it contains.

Ionic liquid Assisted Nanofabrication of Ferromagnetic Co-doped La-Ce Ferrites

Preet Shikha, Tejwant Singh Kang^{*}, B.S. Randhawa^{*}

*Department of Chemistry, UGC-Centre for advanced Studies-I, Guru Nanak Dev University,
Amritsar-143005, India*

Co (II) doped La-Ce ferrite nanoparticles (NPs) ($\text{La}_{0.9}\text{Ce}_{0.1}\text{Fe}_{1-x}\text{Co}_x\text{O}_3$) have been prepared via hydrothermal route using ionic liquid surfactant (1-hexadecyl-3-methyl imidazolium chloride, $[\text{C}_{16}\text{mim}][\text{Cl}]$) as structure directing agent. The synthesized NPs have been characterized by XRD, Raman and IR spectroscopic techniques for structural elucidation. XRD studies revealed the formation of mixed Orthorhombic and Rhombohedral phase with Co doping. The idea about distortion of crystal structure of prepared NPs has been gained by shift of XRD peaks along with change in interplanar distance by the incorporation of dopant. UV-Vis studies have indicated the modification in optical properties of La-Ce ferrites upon doping with Co. Scanning (SEM) and Transmission electron microscopy (TEM) have shed light on the size and morphology of prepared NPs. The doped NPs have been established to be ferromagnetic in nature as revealed by magnetic studies.

Keywords: Doping, Ionic liquid surfactant, Structural distortion, Magnetic properties.

^{*}Corresponding author. Tel.: +91 183 2258802-Ext-3207; Fax: +91 183 225820.

Email address: balwinderrandhawa@gmail.com, tejwantsinghkang@gmail.com

1. Introduction

The phenomenon of doping has upsurge interest in material science and in general, it leads to materials with superior physico-chemical properties as compared to that of undoped nanomaterials. The unique characteristics of transition metal ions such as variable oxidation states, partially filled d-orbitals and their magnetically active nature makes them suitable dopants in various inorganic oxides [1]. The quality and quantity of the dopant significantly affects the physico-chemical properties of doped nanomaterials. LaFeO₃ nanoparticles (NPs) with perovskite structure have been extensively investigated as a powerful candidate for its application in diverse technical avenues such as in sensors, as magnetic materials, as catalyst, in solid oxide fuel cell and as electrode materials etc [2-16]. Due to their flexible crystallographic structure, it is easy to incorporate various dopants to modulate their physico-chemical properties [17]. In this regard, reports are available in literature, where metal ions of different groups like alkali, alkaline earth and transition metals has been incorporated in LaFeO₃ to modulate its physico-chemical properties [18-27]. Most of the reports mentioned above generally discuss about their improvement in their catalytic and sensing behavior, however studies regarding the modulation or improvement in their magnetic behavior with doping are rarely available in literature [28-33]. On the other hand, numerous synthetic routes have been exploited to synthesize nanocrystalline LaFeO₃, which includes solid state reaction of metal oxide, co-precipitation route, precursor method, sol-gel and hydrothermal method [34-38]. Hydrothermal synthesis is one of the techniques employed for the synthesis of nanomaterials where the nucleation, growth and aging of the NPs can be controlled [38]. There are, some reports existing in literature, where synthesis of pure or doped LaFeO₃ materials by hydrothermal route has been carried out. For example *Ponpandian et.al* have synthesized photocatalytic active LaFeO₃ nanostructures of different morphology by facile hydrothermal process [39] and in other report dendritic LaFeO₃ nanostructures for selective determination of Dopamine has also been synthesized via surfactant (CTAB) assisted hydrothermal route [40]. Similar work has been performed to obtain photocatalytically active microspheres composed of LaFeO₃ NPs by hydrothermal method [41]. Regarding doped LaFeO₃, *Feng et.al.* reported the hydrothermal synthesis of LaFe_{1-x}Cr_xO₃ to study their composition dependent magnetic properties [42]. *Dai et.al.* have evaluated the catalytic activity for toluene combustion by porous LaFeO₃ synthesized via glucose assisted

hydrothermal route [43] Now days, a new class of surfactant called as ionic liquid surfactants (ILSs) are gaining immense scientific attraction due to their better surface activity and unique physico-chemical properties over conventional surfactants [44, 45]. In this regard, our research group is also engaged in synthesis and characterization of a variety of ILSs [46-48]. ILSs have been used as a soft template under hydrothermal condition for the controlling the size and morphology of the NPs [49-51]. Although there are many reports regarding the synthesis of LaFeO_3 via hydrothermal route using different structure directing agents, however, there is no report regarding the synthesis of doped LaFeO_3 NPs by hydrothermal route using imidazolium based ILSs as structure directing templates. Even though the other methods like sol-gel, combustion, co-precipitation *etc.* as reported in literature are equally effective and economical routes for the synthesis of pure and doped NPs, but these methods generally gives spherical NPs with insignificant anisotropy [19, 52-58]. Therefore, we have tried ILS assisted hydrothermal route for preparation of Co doped La-Ce ferrite NPs in expectation of synthesizing anisotropic NPs with improved physicochemical properties exploiting the surfactant like nature of used ILS. Here in, we have synthesized and characterized the Co (II) doped $\text{La}_{0.9}\text{Ce}_{0.1}\text{Fe}_{1-x}\text{Co}_x\text{O}_3$ ($x=0, 0.1, 0.3, 0.5$) NPs via hydrothermal route using ILS (1-hexadecyl-3-methyl imidazolium chloride, $[\text{C}_{16}\text{mim}][\text{Cl}]$). To best of our knowledge, this is the first report, where the presence of small content of Ce^{3+} ion along with effect of Co doping at Fe-site of LaFeO_3 NPs is synthesized by hydrothermal route using ILS as structure directing template. In this work, the impact of Co doping on the structural, morphological, optical and magnetic properties of prepared NPs have been investigated in detail.

2. Experimental

2.1 Methodology

For hydrothermal synthesis, stoichiometric quantities of $\text{La}(\text{NO}_3)_3 \cdot 6\text{H}_2\text{O}$, Cerium (III) acetate, $\text{Fe}(\text{NO}_3)_3 \cdot 9\text{H}_2\text{O}$ and $\text{Co}(\text{NO}_3)_2 \cdot 6\text{H}_2\text{O}$ were dissolved in 0.05 M aqueous solution of ionic liquid, 1-hexadecyl-3-methyl imidazolium chloride $[\text{C}_{16}\text{mim}][\text{Cl}]$, which was synthesized and characterized using well established protocol [59]. The obtained mixture was sonicated for 30 min to get a clear solution followed by addition of NaOH required for the complete precipitation of metal ions. The resulting suspension was again sonicated for 15

min for proper mixing and then transferred to teflon-lined stainless steel vessel and autoclaved at 180°C for 24 hrs in an oven. The autoclave was then cooled naturally and the obtained product was washed with distilled water and ethanol to remove the excess base and excess surfactant. The obtained product was dried in air and then grinded followed by calcination at 700 °C for 4-5 hrs.

2.2 Characterization

X-ray diffractograms of the synthesized NPs ($\text{La}_{0.9}\text{Ce}_{0.1}\text{Fe}_{1-x}\text{Co}_x\text{O}_3$) for phase analysis were recorded using a Rigaku Xpert Pro X-ray diffractometer provided with Cu $K\alpha$ radiation (1.541Å) in the 2θ range of 20°-80° at a step size of 0.02°. The average particle size was calculated based on XRD patterns using Scherrer's formula. Raman spectra were obtained for the prepared samples using Renishaw Raman spectrophotometer equipped with 488 and 514 nm Ar-ion laser in the range of 100-2000 cm^{-1} . UV-Vis spectra were recorded on UV-spectrophotometer (UV-1800 SHIMADZU). Magnetic studies were carried out at room temperature in the applied magnetic field of -20 to +20 kOe using Microsense EV-90 vibrating sample magnetometer. The surface morphology of the NPs was investigated by dispersing the sample in ethanol using Zeiss Ultra 55-Limited edition scanning electron microscope. Transmission electron microscope (TEM) images were recorded using JEM-2100 transmission electron microscope at a working voltage of 200 kV. The NPs were dispersed into ethanol using ultrasonicator for sample preparation of TEM measurement. A drop of dispersion was placed on the carbon coated grid (300 Mesh) and excess solution was blotted off. The samples were dried at room temperature for 24 hours before the measurement.

3. Result and Discussion

3.1 XRD analysis

Structural analysis of the prepared nanomaterials has been performed obtaining XRD patterns of synthesized nanomaterials and is shown in Fig. 1(a). XRD spectra of pure and Co doped $\text{La}_{0.9}\text{Ce}_{0.1}\text{Fe}_{1-x}\text{Co}_x\text{O}_3$ NPs indicate the Pervoskite phase having orthorhombic structure, which is consistent with pure LaFeO_3 (JCPDS no. 37-1493). From XRD studies, a change in interplanar (d) value with Co doping for main (121) peak has been observed, which suggests

a change in crystal lattice. Here a transition from Orthorhombic to Rhombohedral phase is assumed to occur as also reported by several researchers [23, 60]. Therefore, newly formed phase of doped samples is assumed to be a mixture of Rhombohedral and Orthorhombic phases. The main diffraction peak (121) in XRD patterns of Co doped samples ($x = 0.3, 0.5$) shows a slight doublet, which is a characteristic signal for Rhombohedral structure [23] as shown in Fig. 1(b), thus confirming the assumption. The average crystallite size of obtained NPs has been calculated by Scherrer's formula and is given in Table 1. As can be seen from Table 1, the Co doping exerts a remarkable effect on crystallite size, which decrease from 23 to 15 nm upon incorporation of Co^{2+} ion. The decrease in crystallite size with Co substitution can be attributed to the lower valence state of Co^{2+} than Fe^{3+} , which can lead to the charge imbalance. This charge imbalance is compensated by formation of oxygen vacancies or change in the valency of metal ions ($\text{Fe}^{3+}/\text{Fe}^{4+}$ or $\text{Co}^{2+}/\text{Co}^{3+}$) leading to hindered growth of NPs [61, 62]. Further, in addition to broadening, a significant shift of XRD peaks towards higher 2θ value has been observed. This can be explained on the basis that replacement of smaller Fe^{3+} ions by larger Co^{2+} ions, results in transformation of orthorhombic to rhombohedral structure or the distortion of the octahedral coordination [63]. There is small peak of La_2O_3 phase appeared in the XRD spectra of undoped La-Ce ferrite, which progressively disappear with Co doping. This suggests that presence of Co^{2+} may stabilize the perovskite phase due to the formation of other Rhombohedral phase of LaCoO_3 in addition to LaFeO_3 . It has been observed that nature and quantity of dopant can modulate the structural parameters of synthesized nanomaterials.

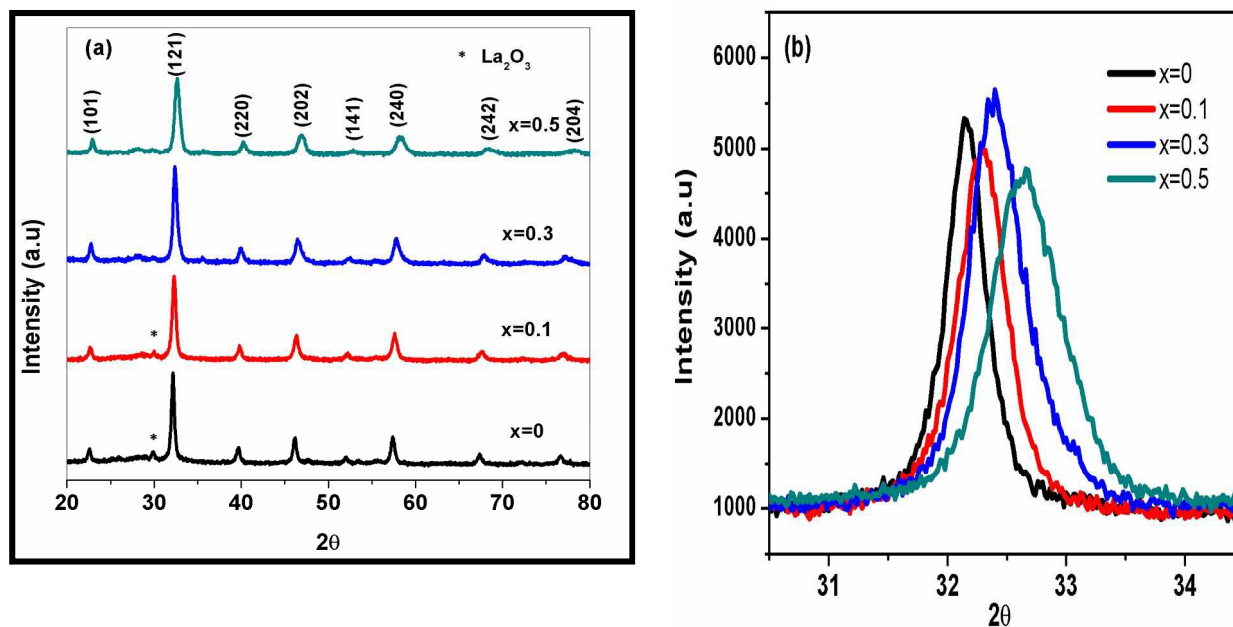


Fig.1. (a) XRD patterns of Co doped $\text{La}_{0.9}\text{Ce}_{0.1}\text{Fe}_{1-x}\text{Co}_x\text{O}_3$ and (b) enlarged view of (121) diffraction peak.

3.2 FTIR & Raman spectroscopic studies

The FTIR spectra of prepared NPs are displayed in Fig.2 (a) and (b). The spectra depicted the strong and broad vibrational bands at ~ 572 and ~ 430 cm^{-1} , which are attributed to the antisymmetric stretching of Fe-O (ν_1) and O-Fe-O deformation vibration (ν_2), respectively, of FeO_6 in octahedral unit of Perovskite ABO_3 [64]. The exact position of vibrational band could not be obtained attributable to broadening of bands, which can be due to both the Fe-O and Co-O stretching vibration in the range of $550\text{-}650$ cm^{-1} [63]. The region of $1200\text{-}1800$ cm^{-1} can be ascribed to the carbonates and bending vibration of bound water molecules, which were present on the surface due to adsorption of CO_2 and H_2O [65]. The absorption of CO_2 indicates the basic nature of surface of synthesized samples. As can be seen from Fig.2, with Co^{2+} substitution, a slight shift of peak ($550\text{-}650$ cm^{-1}) towards higher wavenumber has been observed with decreased broadening thus indicating the structural distortion upon introduction of Co^{2+} ion by affecting the Fe-O bond strength [63]. The decreased broadening at $x=0.5$ shows that Co-O stretching frequency gets prominent at higher doping as compared to Fe-O or O-Fe-O.

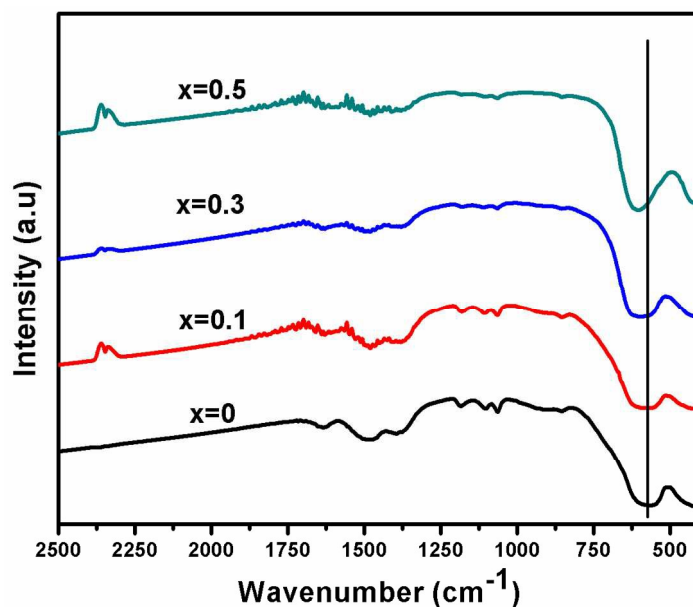


Fig.2. FTIR spectra of Co doped La-Ce ferrite nanoparticles.

On the other hand, Raman spectroscopy is a powerful technique, which provide chemical fingerprint of specific compound or material. Most of the metal oxides show metal-oxygen vibration frequencies in the range of 200-1000 cm^{-1} , where Raman spectroscopy may clearly be the choice over FTIR spectroscopy. The effect of substitution of Co in La-Ce ferrites is expected to induce some structural defects, which can be easily analyzed by Raman studies. Fig.3 (a) and (b) shows the Raman spectra of Co doped La-Ce ferrites NPs by using a laser of wavelength 514 and 488 nm, respectively. The undoped La-Ce ferrite shows bands at 148, 222, 287, 422, 540 and 643 cm^{-1} which are in agreement with the literature [66, 67]. At low content of Co^{2+} ($x=0.1$), number of Raman bands has been found to be decreased due to merging of peaks and a broad band in the region of 400-800 cm^{-1} with increase in intensity around 630 cm^{-1} as compared to undoped La-Ce NPs has been observed. This supports the substitution of Co^{2+} ion in lattice of LaFeO_3 . The increase in intensity of Raman band with slight doping ($x=0.1$) can be the result of substitutional disorder, which may cause bond length fluctuation [68]. This suggests that Co^{2+} is affecting the oxygen tilt and hence, stretching and bending modes of vibration. At higher doping of Co ($x=0.3, 0.5$), we could not observe any Raman bands with 514 nm Ar ion laser, but with 488 nm laser, a less intense and broadened band around 630 cm^{-1} has appeared. This behavior can be due to the fluorescent effect at excitation wavelength of 488 nm or can be attributed to the doping effects, which cause structural disorder. The Raman band in the vicinity of 630 cm^{-1} due

to two phonon or impurity-related scattering are frequently observed in the perovskite-type structure [69]. Structural modifications in the crystal lattice by Co substitution as revealed by XRD studies can also be judged by Raman studies. As can be seen from the spectra, the doped samples show somewhat different behavior than that of undoped La-Ce ferrite NPs. Thus from the XRD, FTIR and Raman studies, it has been observed that Co doping in La-Ce ferrites leads to structural distortion either by change in the valence state or creating oxygen deficiency. The change in physico-chemical properties induced by Co doping in La-Ce ferrite are also reflected in various studies as discussed in later sections.

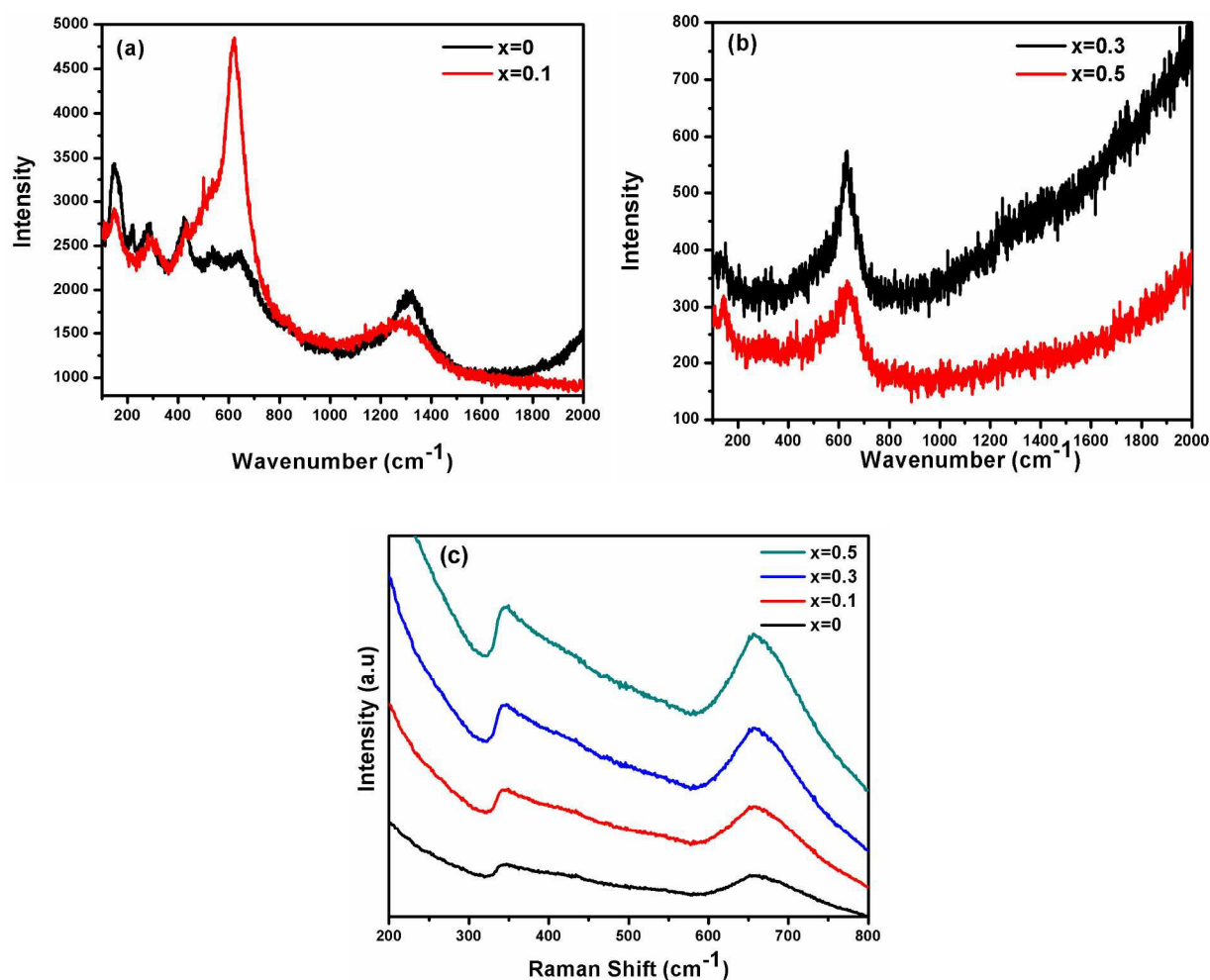


Fig.3. Raman spectra of Co doped La-Ce ferrites nanoparticles (a) excitation wavelength 514 nm (b) 488 nm (c) 785 nm.

To have better insights and proper comparison of Raman spectra, the Raman spectra of Co doped La-Ce ferrites NPs has been obtained at excitation wavelength of 785 nm and shown in Fig.3c.

The samples show different behavior than that observed at excitation wavelength of 488 and 514 nm. Here, the intensity of Raman bands also increases with Co doping along with prominent broadening with a slight shift of bands towards lower frequency, which could be due to the decrease in average particle size with Co doping. This increased line width of the bands in spectra with doping can be attributed to the substitutional disorder or due to phonon scattering from randomly distributed cations in the lattice. The distortion of bond angles may also destroy the long range order but nearest neighbor interaction are affected that leads to a shift in vibrational frequency [68].

3.3 UV-Vis Studies

UV-Vis studies have been carried out on Co-doped La-Ce ferrites NPs to explore the electronic properties and absorbance behavior of synthesized samples. Fig.4 shows that all the NPs shows absorbance in UV-Vis region in the range of 250-580 nm with prominent band centered on 325 and 470 nm. The electronic transition from valence band to conduction band ($O_{2p} \rightarrow Fe_{3d}$) is mainly responsible for strong absorption band in perovskite type oxide [69, 70]. With Co doping, a red shift mainly in visible region (from 426 to 475 nm) in absorption spectra has been observed, which indicates that doping leads to the change in optical properties of synthesized NPs. The slight red shift in absorption spectra can be correlated with decrease in band gap with doping. Thus decrease in band gap with Co doping in La-Ce Ferrites can be exploited for photocatalytic and sensing applications by harvesting more photons of light to excite the electrons from the valence band to the conduction band.

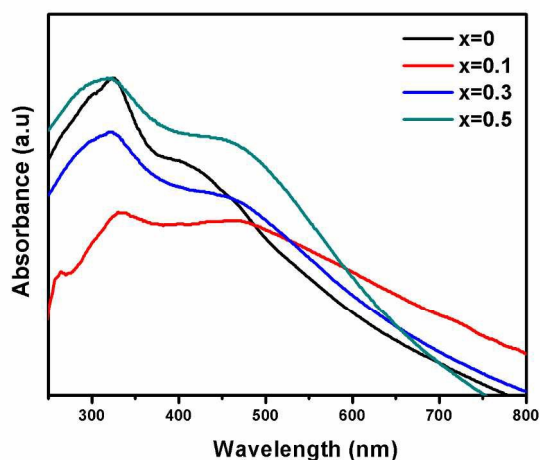


Fig.4. UV-Vis spectra (normalized) of Co Doped La-Ce ferrites nanoparticles.

3.4 Morphological studies

Fig.5 shows the SEM images of the synthesized pure and Co doped La-Ce ferrite NPs. The morphology of the obtained sample ($x=0$) appeared to be the mixture of aggregated rod-like and spherical structures. The SEM images of Co doped samples don't indicate the clear morphology because of some aggregation due to their enhanced magnetic nature than that of undoped NPs as established from magnetic studies discussed in later section (Section 3.5). However, TEM images provide clear view of shape and size of Co doped NPs as shown in Fig.7. The shape of undoped La-Ce ferrite NPs ($x=0$) appear to be an interconnecting rod like assembly of spherical NPs as can be seen from Fig. 7. The change in morphological properties of prepared nanomaterials could be due to effect of concentration of precursor or template. To get insight into this phenomenon, different concentration of ILS (0, 10, 50 and 200mM) has been employed at a constant concentration of precursor (3mmol). The TEM images of thus obtained NPs are provided in Fig.8. It has been found that in the absence of ILS the obtained La-Ce ferrite NPs show spherical morphology with aggregation, however, at low concentration of ILS (10mM), mainly spherical NPs clubbed with each other via sheet like architectures has been obtained. At higher content of ILS *i.e.* at 50 and 200 mM, a network of elongated rod like NPs along with some spherical NPs has been obtained. This shows that with the increase in concentration of ILS, a change in morphology from spherical to rod like along with varying extent of aggregation of NPs takes place and the morphology of prepared NPs is dominantly controlled by the presence of template. No significant change in XRD pattern has been obtained, but a slight increase in average crystallite size of NPs with increase in the concentration of ILS has been observed as can be seen from Table S1 (supplementary information). Thus we have concluded that the presence of ILS in the reaction medium creates some anisotropy in the NPs, where aggregated spherical NPs are observed in the absence of ILS. Co doping (at a fixed concentration of ILS at 50 mM) in La-Ce ferrite NPs does not significantly influence the morphology of prepared NPS, however, it exerts affect on physico-chemical properties of prepared NPs. The NPs obtained at lower content of Co^{2+} ion ($x=0.1$) shows some dendrites/rods like morphology, which can be a result of templating effect of ILS. The particles are interacting with each other due to their weak magnetic

nature. For higher content of Co-doped samples ($x=0.5$), there is an increase in the aggregation of the nanomaterials as observed from TEM analysis.

Morphology and size of NPs is generally controlled by various internal and external factors. The use of surfactants has been commonly employed for controlling the morphology and size of the NPs. Among them IL based surfactants having imidazolium moiety has unique directional ability due to extended hydrogen bond network. In this work, we have used the $[C_{16}mim][Cl]$ as surfactant along with Co doping to synthesize and investigate their effect on morphology and physico-chemical properties of obtained NPs. Scheme.1 illustrates the forming mechanism of pure and doped NPs. The strong tendency of $[C_{16}mim][Cl]$ to self-aggregate into ordered structures, which have a large steric hindrance thus can provide space for oriented arrangement of growing NPs in 2D direction [71]. The self-assembled structure of ILS such as micelles present in solution templating the forming NPs are expected to come closer due to magnetic interaction between NPs in an elongated fashion. The growth of NPs here takes place in such 2D structures, where aggregation of NPs mediated by ILS takes place resulting in a rod like morphology having some spherical structure. The shape of micelles formed by ILS may get affected by the addition of Co^{2+} ion as a dopant similar to that of additive in ionic surfactant solution [72], which could influence the growth of NPs thus can affect the morphology of obtained NPs. The self-assembled NPs forms an interconnected network on calcination, which can be due to magnetic interaction among the doped NPs as observed in SEM and TEM images. The presence of Co^{2+} in the sample may hinder the growth of NPs as observed from the decrease in average crystallite size from XRD studies and thus complete rod like network has not been observed as obtained for undoped NPs. The doping of Co^{2+} in La-Ce ferrites NPs at fixed concentration of ILS (50 mM) leads to aggregation of rod and spherical NPs due to the magnetic interaction among the NPs, thus cluster like network has been observed in TEM images of doped samples. The particle size and morphology of the obtained samples synthesized by our method has been compared with the other methods in literature and displayed in Table 2. EDX analysis of the pure and doped NPs as shown in Fig.6 confirms the presence of La, Fe, Ce, Co and O elements in appropriate amounts. The HRTEM images shown in Fig.7 provide further information about the change in interplanar distance with Co doping in La-Ce ferrites NPs. The lattice fringes spacing of the undoped NPs is 0.28 nm, which is well indexed with the (121) plane of orthorhombic structure. With Co doping a slight decrease from 0.28 nm to 0.267 nm in the “d”

spacing of the lattice fringes has been observed, which can be correlated with the XRD studies thus suggesting some structural distortion with doping.

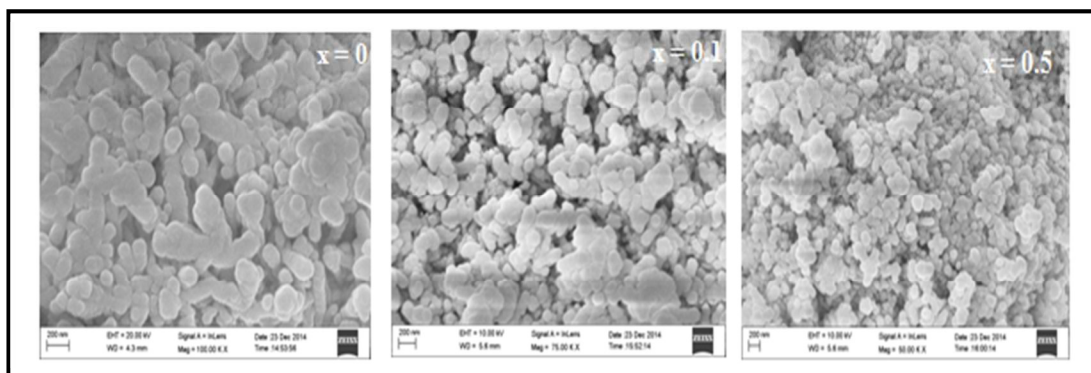


Fig.5. SEM images of Co doped $\text{La}_{0.9}\text{Ce}_{0.1}\text{Fe}_{1-x}\text{Co}_x\text{O}_3$ nanoparticles.

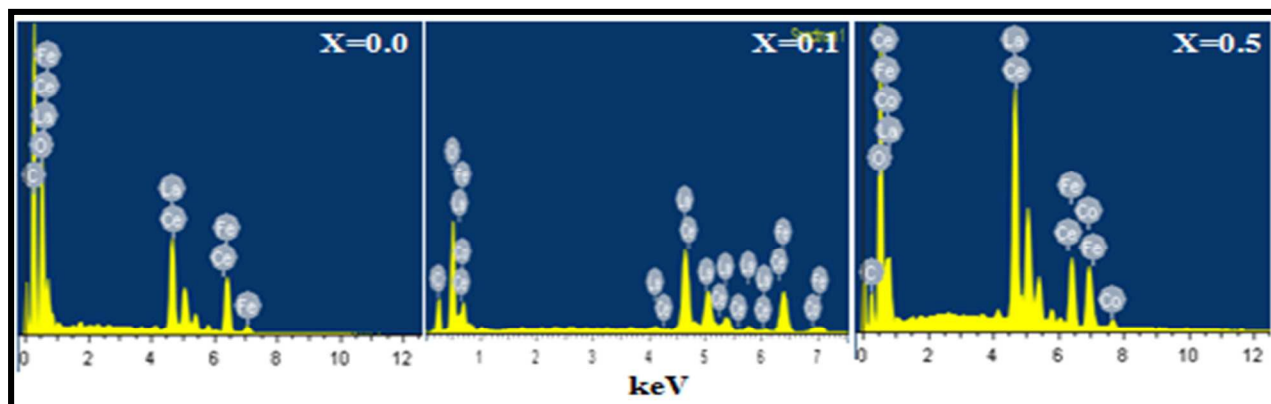


Fig.6. EDX spectra of Co doped $\text{La}_{0.9}\text{Ce}_{0.1}\text{Fe}_{1-x}\text{Co}_x\text{O}_3$ nanoparticles.

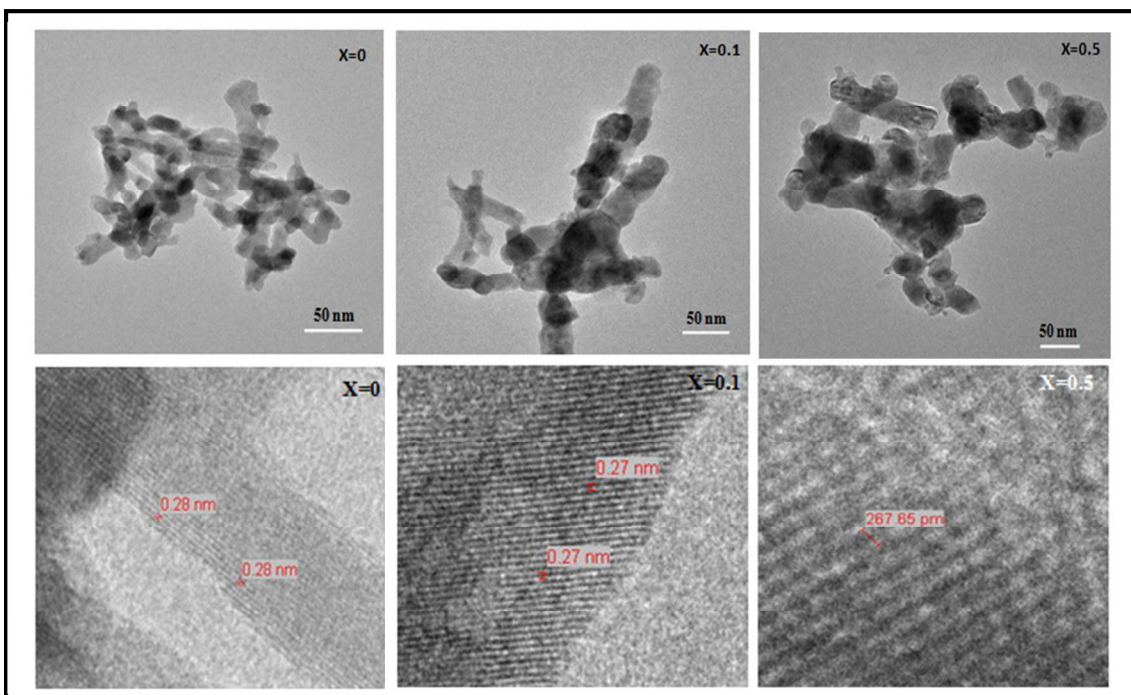


Fig.7. TEM (above) and HRTEM (below) images of Co doped $\text{La}_{0.9}\text{Ce}_{0.1}\text{Fe}_{1-x}\text{Co}_x\text{O}_3$ nanomaterials.

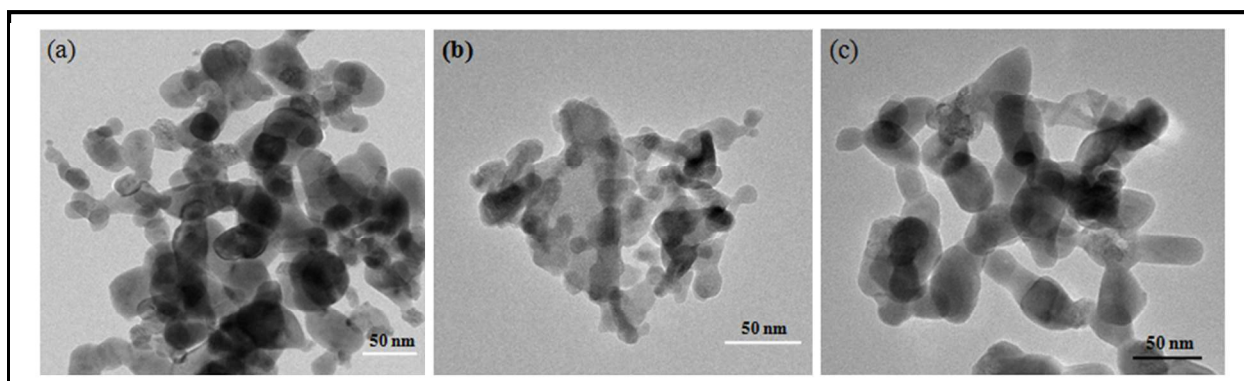


Fig.8. TEM images of undoped La-Ce ferrite NPs obtained from different conc. of ILS (a) 0mM (b) 10 mM (c) 200 mM.

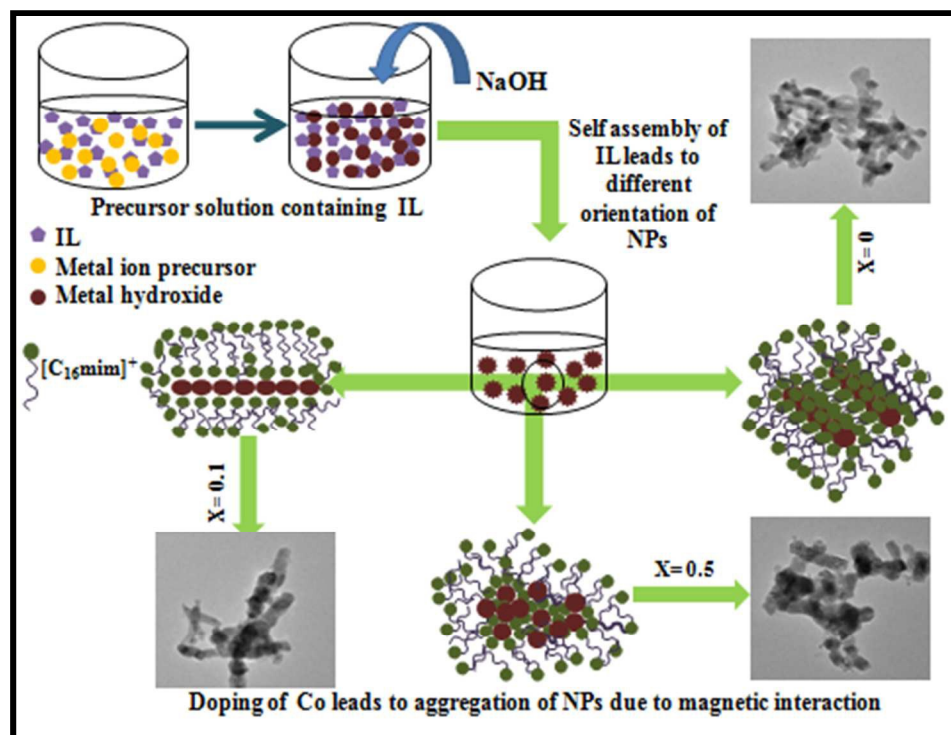
Table 1. Physico-chemical parameters of Co doped $\text{La}_{0.9}\text{Ce}_{0.1}\text{Fe}_{1-x}\text{Co}_x\text{O}_3$ nanomaterials at room temperature synthesized by hydrothermal route.

| Co content (x) in $\text{La}_{0.9}\text{Ce}_{0.1}\text{Fe}_{1-x}\text{Co}_x\text{O}_3$ | Average Crystallite size from XRD (nm) | Particle size from TEM (nm) | Saturation Magnetization (M_S) (emu/g) | Remnant Magnetization (M_R) (emu/g) | Coercivity (H_c) (Oe) |
|--|--|-----------------------------|--|---|---------------------------|
| 0.0 | 23.1 | 15-25 | 0.123 | 0.0075 | 569.4 |
| 0.1 | 18.2 | 25-35 | 2.233 | 0.1489 | 119.4 |
| 0.3 | 15.8 | ----- | 3.297 | 0.7727 | 231.0 |
| 0.5 | 15.2 | 30-40 | 2.403 | 0.3187 | 124.9 |

Table 2. Comparison of morphology of La-based ferrite NPs (pure or doped) prepared in present work with that reported in literature.

| Sr.No. | Sample | Synthetic Route | Template /surfactant | Morphology obtained | Particle Size (nm) | Ref. |
|--------|--------------------|---------------------------------|----------------------------------|------------------------|--------------------|----------------|
| 1. | La-Ce ferrite | Hydrothermal route | ILS [C ₁₆ mim][Cl] | Interconnecting rods | 15-25 | This work |
| 2. | LaFeO ₃ | Hydrothermal route | ILS [C ₁₆ mim][Cl] | Spherical and rods | 18-28 | This work (SI) |
| 3. | LaFeO ₃ | Glycine combustion | ----- | Irregular spherical | 57-59 | [52] |
| 4. | LaFeO ₃ | Gel -based auto combustion | ----- | Agglomerated Spherical | 60-80 | [53] |
| 5. | LaFeO ₃ | Reverse microemulsion | Aerosol-OT, AOT | Spherical | 24.65 | [56] |
| 6. | La-Ce ferrite | Sol-gel | ----- | Spherical | 25-37 | [19] |
| 7. | La-Ce ferrite | Combustion and Co-precipitation | ----- | Spherical | 24-27 | [54] |
| 8. | LaFeO ₃ | Sonochemical | ----- | Agglomerated particles | 30 | [55] |

| | | | | | | |
|-----|--------------------|---------------------|----------------|---------------------|-------|------|
| 9. | LaFeO ₃ | Non-aqueous | Benzyl alcohol | | | [57] |
| 10. | LaFeO ₃ | Polymerized-complex | ----- | Irregular Spherical | 44-74 | [58] |



Scheme.1. Probable mechanism for the formation of pure and Co doped La-Ce ferrites NPs.

3.5 Magnetic studies

Magnetic properties of the Co doped La-Ce Ferrites NPs at room temperature have been investigated using vibrating sample magnetometer. LaFeO₃ are generally antiferromagnetic (canted) in nature. In LaFeO₃, the superexchange interaction between two Fe³⁺ ions through the intervening oxide ions results in its antiferromagnetic nature, however due to slight canting of spins, a weak ferromagnetism has been observed [73]. The antiferromagnetic/weak ferromagnetic nature of LaFeO₃ NPs limits their application in magnetic devices, therefore need of hour is to increase their magnetization. Their magnetic properties are usually influenced by the choice of synthetic route and type of doping [28-33]. The effect of Co doping on the

magnetic properties of synthesized nanomaterials are shown in Fig. 9(a) and (b). The presence of hysteresis loop indicates the existence of weak ferromagnetic character at room temperature. The various magnetic parameters such as coercivity (H_C), remnant (M_R) and saturation (M_S) magnetization as a function of Co content are provided in Table 1. Co doping in La-Ce ferrite leads to the significant enhancement in various magnetic parameters up to a certain extent i.e upto $x=0.3$. The drastic change has been observed in M_S with Co doping (3.297emu/g) as compared to undoped ferrites sample (0.123emu/g). The probable reasons for such behavior seem to be structural distortion caused by doping, which weakens the superexchange interactions by changing the canting angle [74]. The particle size reduction with doping can also affects the magnetic properties by increasing the uncompensated spins on the surface [75]. Addition of Co upto certain extent ($x=0.3$) enhances the magnetic parameters (M_R and M_S), which further goes on decreasing at higher doping. Suitable reasons for this observation is that with the addition of Co ion, the superexchange interactions among $Fe^{3+}-O-Fe^{3+}$ are replaced by some $Fe^{3+}-O-Co^{2+}$ at intermediate doping. Due to the different electronic arrangement of Co and Fe ions, complete cancellation of their spins is prevented and thus sample show enhanced magnetization than undoped sample at room temperature [76, 77]. But at higher doping ($x=0.5$), in addition of $LaFeO_3$ phase, formation of some $LaCoO_3$ phase takes place as revealed by XRD, which has $Co^{2+}-O-Co^{2+}/Co^{3+}-O-Co^{3+}$ interactions that can coupled antiferromagnetically, leading to slight reduction in M_R and M_S .

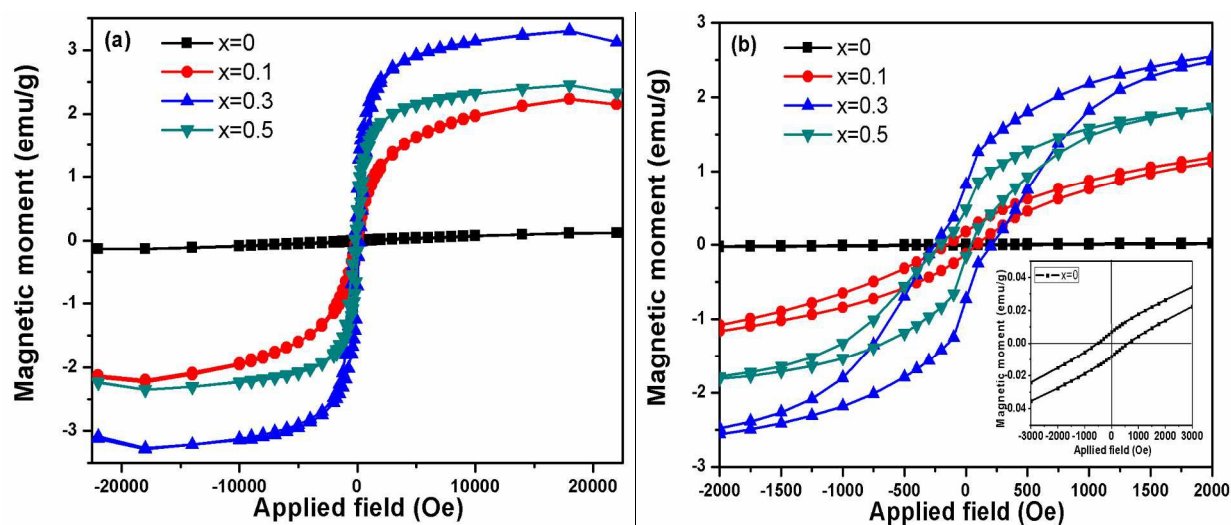


Fig.9 (a) Hysteresis loops of Co doped La-Ce ferrite nanoparticles at room temperature **(b)** Magnified view of Fig.9 (a) in lower applied field.

The variation in H_C as a function of Co content in La-Ce ferrites is shown in Fig.10. The undoped NPs shows the highest H_C , which first decreases and then increases upto certain extent of doping ($x=0.3$). The large H_C observed in undoped La-Ce NPs can be attributed to the shape anisotropy as observed in TEM image, which has some interconnecting rod like appearance thus results in higher H_C [78] whereas La-Ce ferrites NPs synthesized by our group via combustion and co-precipitation shows low H_C [54]. This shows some anisotropic effect induced by ILS on the synthesized NPs. The structural transition at higher doping of Co ($x=0.5$) can also not be ruled out as a reason behind decrease in various magnetic parameters as revealed from XRD studies. Thus enhanced magnetization of LaFeO_3 type oxides by doping can be utilized for variety of applications, which can further be controlled under the application of magnetic field.

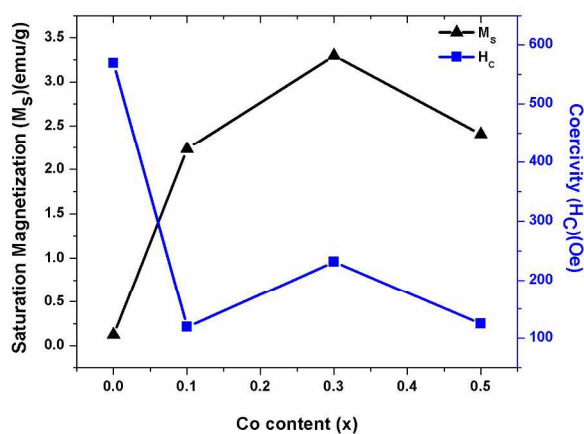


Fig.10. Variation of M_s and H_C with Co doping.

Further, the motive to use the ILS is to provide some directional property to the synthesized NPs, which generally is not found with other methods like citrate gel and combustion method etc, where mostly small aggregated spherical NPs with minor or insignificant anisotropy as observed from literature survey [52-58]. However due to lack of literature regarding magnetic studies of Co doped La-Ce ferrites NPs exact comparison could not be done.

Conclusion

The impact of Co doping on physico-chemical properties of La-Ce ferrites NPs synthesized by hydrothermal route using ILS (1-hexadecyl-3-methyl imidazolium chloride, $[\text{C}_{16}\text{mim}][\text{Cl}]$) have been investigated. The information obtained from XRD and IR studies indicates the structural transition with decrease in average crystallite size (15-23 nm) with Co doping due to charge

imbalance. The amount of Co doping has been found to induce structural distortion and thus control the physico-chemical properties of La-Ce ferrite NPs. The obtained ferrites show mixture of rods and spherical NPs thus giving an appearance of partial dendrite like structure. Magnetic parameters such as saturation magnetization were significantly enhanced (from 0.123 to 3.297 emu/g) with Co doping ($x=0.3$) as compared to undoped ferrite NPs due to more uncompensated surface spins on the surface of NPs and due to different magnetic moment of dopant. In a nutshell, physico-chemical properties specifically magnetic properties of La-Ce ferrites NPs have been significantly improved with Co doping synthesized via ILS-assisted hydrothermal approach.

Acknowledgement

The authors are very thankful to the Council of Scientific and Industrial Research (CSIR), New Delhi, India, vide Project number 01/(2774)/14-EMR-II and Defence Research and Development Organization (DRDO), project number ERIP/ER/1003912/M/01/1417, New Delhi, India for financial support.

References

1. The Organometallic Chemistry of the Transition Metals, Robert H. Crabtree, John Wiley and Sons, Apr 2009.
2. H. Obayashi, Y. Sakurai and T. Gejo, *J. Solid State Chem.*, 1976, **17**, 299–303.
3. P. Song, H. W. Qin, L. Zhang, K. An, Z. J. Lin, J. F. Hu and M. H. Jiang, *Sens. Actuators B*, 2005, **104**, 312–316.
4. T. V. Choudhary, S. Banerjee and V. R. Choudhary, *Appl. Catal. A*, 2002, **234**, 1–23.
5. L. G. Tejuca, and J. Less, *Common Met.*, 1989, **146**, 261–270.
6. Y. Teraoka, M. Yoshimatsu, N. Yamazoe and T. Seiyama, *Chem. Lett.*, 1984, **13**, 893–896.
7. H. Fal on, M. J. Martinez-Lope, J. A. Alonso and J. L. G. Fierro, *Appl. Catal. B*, 2000, **26**, 131–142.
8. O. Mihai, D. Chen and A. Holmen, *Ind. Eng. Chem. Res.*, 2011, **50**, 2613–2621.

9. O. Mihai, D. Chen and A. Holmen, *J. Catal.*, 2012, **293**, 175–185.
10. F.J. Berry, X. Ren, J.R. Ganced and J.F. Marco, *Hyperfine Interact.*, 2004, **156**, 335–340.
11. Q. Zhang and F. Saito, *J. Mater. Sci.*, 2001, **36**, 2287–2290.
12. S. Nakayama, *J. Mater. Sci.*, 2001, **36**, 564–5648.
13. Q. Ming, M.D. Nersesyan, A. Wagner, J. Ritchie, J.T. Richardson, D. Luss, A.J. Jacobson and Y.L. Yang, *Solid State Ionics.*, 1999, **122**, 113–121.
14. T. Arakawa, H. Kurachi and J. Shiokawa, *J. Mater. Sci.*, 1985, **20**, 1207–1210.
15. Y. Shimizu, M. Shimabukuro, H. Arai and T. Seiyama, *Chem. Lett.*, 1985, **14**, 917–920.
16. G. Martinelli, M.C. Carotta, M. Ferroni, Y. Sadaoka, E. Traversa, *Sens. Actuators. B*, 1999, **55**, 99–110.
17. A. Manthiram, J. H. Kim, Y. N. Kim and K. T. Lee, *J. Electroceram.*, 2011, **27**, 93-107.
18. Y. Chen, H.M. Yuan, G. Tian, G.H. Zhang, S.H. Feng, *J. Solid State Chem.*, 2007, **180**, 167–172.
19. X.P. Xiang, L.H. Zhao, B.T. Teng, J.J. Lang, X. Hu, T. Li, Y.A. Fang, M.F. Luo and J.J. Lin, *Appl. Surf. Sci.*, 2013, **276**, 328–332.
20. L. Hou, G. Sun, K. Liu, Y. Li and F. Gao, *J. Sol-Gel Sci. Technol.*, 2006, **40**, 9–14.
21. M. Ghasdia, H. Alamdaria, S. Royerb and A. Adnot, *Sensors and Actuators. B*, 2011, **156**, 147–155.
22. Y. Sun, S.S. Hla, G.J. Duffy, A.J. Cousins, D. French, L.D. Morpeth, J.H. Edwards and D.G. Roberts, *International Journal of Hydrogen Energy.*, 2011, **36**, 79-86.
23. M. M. Natile, F. Poletto, A. Galenda, A. Glisenti, T. Montini, L. D. Rogatis, and P. Fornasiero, *Chem. Mater.*, 2008, **20**, 2314–2327.
24. M. V. Kuznetsov, Q. A. Pankhurst, I. P. Parkinc and Y. G. Morozova *J. Mater. Chem.*, 2001, **11**, 854-858.
25. S. Dong, K. Xu, G. Tian, *J Mater Sci.*, 2009, **44**, 2548–2552.
26. H. Wu, R. Hu, T. Zhou, C. Li, W. Meng and J. Yang, *Cryst Eng Comm.*, 2015, **1**, 3859–3865.
27. H.A. Medkhali, K. Narasimharao, S. N. Basahel and M. Mokhtar, *Journal of Membrane and Separation Technology.*, 2014, **3**, 206-212.

28. R. J. Choudhary, R. Kumar, M. W. Khan, J. P. Srivastava, S. I. Patil, S. K. Arora and I. V. Shvets, *Appl. Phys. Lett.*, 2005, **87**, 132104.
29. L. Yuan, K. Huang, C. Hou, W. Feng, S. Wang, C. Zhou and S. Feng, *New J. Chem.*, 2014, **38**, 1168.
30. M. A. Ahmed, N. Okasha and B. Hussein, *J. Alloys Compd.*, 2013, **553**, 308–315.
31. D.V. Karpinsky, I.O. Troyanchuk, K. Bärner, H. Szymczak and M. Tovar, *J. Phys. Condens. Matter.*, 2005, **17**, 7219–7226.
32. Y. Janbutrach, S. Hunpratub and E. Swatsitang, *Nanoscale Research Letters.*, 2014, **9**, 498.
33. K. Mukhopadhyay, A.S. Mahapatra and P.K. Chakrabarti, *Journal of Magnetism and Magnetic Materials.*, 2013, **329**, 133–141.
34. M. Shi, N. Liu, Y. D. Xu, C. Wang, Y. P. Yuan, P. Majewski and F. Aldinger, *J. Mater. Process. Technol.*, 2005, **169**, 179–183.
35. J. J. Liang and H. S. Weng, *Ind. Eng. Chem. Res.*, 1993, **32**, 2563–2572.
36. S. Royer, F. Bérubé and S. Kaliaguine, *Appl. Catal. A*, 2005, **282**, 273–284.
37. A. E. Giannakas, A. K. Ladavos and P. J. Pomonis, *Appl. Catal. B*, 2004, **49**, 147–158.
38. K. Byrappa and T. Adschiri, *Progress in Crystal Growth and Characterization of Materials.*, 2007, **53**, 117-166.
39. S. Thirumalairajan, K. Girija, Neha Y. Hebalkar, D. Mangalaraj, C. Viswanathan and N. Ponpandian, *RSC Adv.*, 2013, **3**, 7549–7561.
40. S. Thirumalairajan, K. Girija, V. Ganesh, D. Mangalaraj, C. Viswanathan, and N. Ponpandian, *Cryst. Growth Des.*, 2013, **13**, 291–302.
41. S. Thirumalairajan, K. Girija, V. Ganesh, D. Mangalaraj, C. Viswanathan, A. Balamurugan and N. Ponpandian, *Chem.Eng. J.*, 2012, **209**, 420–428.
42. W. Hu, Y. Chen, H. Yuan, G. Zhang, G. Li, G. Pang and S. Feng, *J. Solid State Chemistry.*, 2010, **183**, 1582–1587.
43. K. Ji, H. Dai, J. Deng, L. Song, S. Xie and W. Han, *J. Solid State Chem.*, 2013, **199**, 164-170.
44. X. Liu, X. Duan, Q. Qin, Q. Wang and W. Zheng, *Cryst Eng Comm.*, 2013, **15**, 3284–3287.

45. A.Z. Hezave, S. Dorostkar, S. Ayatollahi, M. Nabipour and B. Hemmateenejad, *Colloids & Surfaces A*, 2013, **421**, 63-71.
46. R. Kamboj, P. Bharmoria, V. Chauhan, G Singh, A. Kumar, S. Singh and T. S. Kang, *Phys.Chem.Chem.Phys.*, 2014, **16**, 26040-26050.
47. R. Kamboj, P. Bharmoria, V. Chauhan, S. Singh, A. Kumar, V. S. Mithu and T. S. Kang, *Langmuir.*, 2014, **30**, 9920-9930.
48. V. Chauhan, R. Kamboj, S. P. S. Rana, T. Kaur, G. Kaur, S. Singh, and T. S. Kang, *J.Colloid Interface Sci.*, 2015, **446**, 263-271.
49. X. Bai, L. Zheng, N. Li, B. Dong and H. Liu, *Cryst. Growth Des.*, 2008, **8**, 3840-3846.
50. J. Ma, X. Liu, J. Lian, X. Duan and W. Zheng, *Cryst. Growth Des.*, 2010, **10**, 2522-2527.
51. K.J. Holmberg, *J.Colloid Interface Sci.*, 2004, **274**, 355-364.
52. Y. Wang, J. Zhu, L. Zhang, X. Yang, L. Lu and X. Wang, *Mater. Lett.*, 2006, **60**,1767.
53. H. Shen, G. Cheng, A. Wu, J. Xu and J. Zhao *Phys. Status Solidi A*, 2009, **206**, 1420-1424.
54. P. Shikha, T. S. Kang and B.S. Randhawa *Journal of Alloys and Compounds.*, 2015, **625**, 336-345.
55. M. Sivakumar, A. Gedanken, W. Zhong, Y. H. Jiang, Y.W.Du, I. Brukental, D. Bhattacharya, Y. Yeshurun and I. Nowik, *J.Mater.Chem.*, 2004, **14**, 764-769.
56. R. Abazari and S. Sanati, *Superlattices and Microstructures.*, 2013, **64**,148-157.
57. W. Yang, R. Zhang, B. Chen, N. Bion, D.Duprez, L. Hou, H. Zhang and S. Royer, *Chem. Commun.*, 2013, **49**, 4923-4925.
58. S. Phokha, S. Pinitsoontorn, S. Maensiri and S. Rujirawat, *J Sol-Gel Sci Technol.*, 2014, **71**, 333-341.
59. K. R Seddon, A. Stark and M. Torres, *J. Pure Appl. Chem.*, 2000, **72**, 2275-2287.
60. I. O. Troyanchuka, D. V. Karpinskiĭ, V. M. Dobryanskiĭ, Yu. A. Fedotova and H. Szymczak, *Journal of Experimental and Theoretical Physics.*, 2005, **6**, 1121-1126.
61. Z. Wang, C. Chen, C. Feng, J. Wang, B. Zou, M. Zhao and F. Wu, *Acta Phys. Chim. Sinica.*, 2008, **24**, 375-378.
62. C. Feng, S. Ruan, J. Li, B. Zou, J. Luo, W. Chen, W. Dong and F. Wu, *Sensors and Actuators B*, 2011, **155**, 232-238.
63. H. Cui, M. Zayat and D. Levy, *J. Non-Cryst. Solids.*, 2006, **352**, 3035-3040.

64. P. Jeevanandam, Y. Kolytyn, O. Palchik and A. Gedanken, *J. Mater. Chem.*, 2001, **11**, 869-873.
65. G. V. S. Rao, C. N. R. Rao and J. R. Ferraro, *Appl. Spectrosc.*, 1970, **24**, 436-445.
66. J. Feng, T. Liu, Y. Xu, J. Zhao, Y. He, *Ceramics International.*, 2011, **37**, 1203–1207.
67. C. Jagadeeshwaran, A. P. Blessington, Selvadurai, V. Pazhanivelu and R. Murugaraj, *International Journal of Innovative Research in Science & Engineering, ISSN (Online)* 2347-3207.
68. Ruchita S. Das and Y.K. Agrawal *Vibrational Spectroscopy* 57 (2011) 163– 176.
69. M. Popa, J. Frantti and M. Kakihana, *Solid State Ionics.*, 2002, **154**, 437–445.
70. K. Li, D. Wang, F. Wu, T. Xie and T. Li, *Mater. Chem. Phys.*, 2000, **64**, 269–272.
71. (a) A. Taubert, *Angew. Chem., Int. Ed.*, 2004, **43**, 5380-5382 (b) Y. Zhou and M. Antonietti, *Adv. Mater.*, 2003, **15**, 1452-1455.
72. Surfactant and interfacial phenomena, 2nd Ed. M.J. Rosen, John Wiley and Sons, New York, 1989.
73. D. Treves, *J Appl Phys.*, 1965, **36**, 1033-1039.
74. W.S. Kim, Y.K. Jun, K. H. Kim and S.H. Hong, *Journal of Magnetism and Magnetic Materials.*, 2009, 321, 3262–3265.
75. L. Neel, *Compt. Rend.*, 1961, 252, 4075.
76. S. Basu, S. K. M. Hossain, D. Chakravorty and M. Pal, *Curr. Appl. Phys.*, 2011, **11**, 976.
77. W.S. Kim, Y. Kijun, K.H. Kim and S. H. Hong, *J. Magn. Magn. Mater.*, 2009, **321**, 3262.
78. H.W. Zhang, T.Y. Zhao, J. Zhang, C.B. Rong, S.Y. Zhang, B.G. Shen, L. Li and L. G. Zhang, *J. Phys. D. Appl. Phys.*, 2003, **36**, 1769-1772.